Eur. Phys. J. C (2025) 85:992
https://doi.org/10.1140/epjc/s10052-025-14716-7

THE EUROPEAN PHYSICAL JOURNAL C



Regular Article - Theoretical Physics

# Revisiting the constraints on interacting holographic dark energy models with current observational data

**Xiaofang Shen**[1], **Bing Xu**[2,a], **Kaituo Zhang**[1,b], **Xiangyun Fu**[3], **Liangliang Ren**[2], **Zelin Zhang**[2]

[1] Department of Physics, Anhui Normal University, Wuhu 241000, Anhui, China
[2] School of Electrical and Electronic Engineering, Anhui Science and Technology University, Bengbu 233030, Anhui, China
[3] Department of Physics, Key Laboratory of Intelligent Sensors and Advanced Sensor Materials, Hunan University of Science and Technology, Xiangtan 411201, Hunan, China

Received: 17 April 2025 / Accepted: 30 August 2025


**Abstract** We update the observational constraints on the interacting holographic dark energy (IHDE) models by considering ten representative interaction forms, each defined in terms of the energy densities of dark energy ($\rho_{\rm de}$) and dark matter ($\rho_{\rm dm}$). This analysis utilizes the latest observational datasets, including baryon acoustic oscillation (BAO) measurements from the second data release (DR2) of the Dark Energy Spectroscopic Instrument (DESI), type Ia supernova (SNIa) data from the full five-year observations of the Dark Energy Survey (DES), cosmic microwave background (CMB) observations from Planck 2018, observational Hubble parameter data (OHD), and the local measurement of Hubble constant. Using AIC, BIC and Bayes factor, we find that the $\Lambda$CDM model remains the most strongly favored by the data, while the holographic dark energy (HDE) model is ruled out. Relative to the HDE model, the IHDE models provide a significantly better fit to the data, and the interaction can help alleviating the Big Rip problem. Among the ten IHDE models considered, the two with interaction terms $Q = 3\beta H_0 \rho_{\rm de}$ and $Q = 3\beta H_0 \sqrt{\rho_{\rm dm}\rho_{\rm de}}$, are the most strongly supported by the observational data, where $\beta$ is the coupling parameter. Additionally, the AIC, BIC, and Bayes factor values for the majority of IHDE models are nearly identical, indicating minimal differences in their fitting performance with the current data. This implies that more precise future observations will be necessary to better distinguish between these interaction forms.

## 1 Introduction

In 1998, two independent supernova (SN) teams, led by A. Riess and S. Perlmutter, discovered that our universe is undergoing an accelerating expansion [1,2]. This finding was later confirmed by a series of observations [3–5]. To explain this cosmic acceleration, cosmologists often introduce a component with negative pressure, known as dark energy (DE) [6], to drive the acceleration. Among the various dark energy models, the $\Lambda$CDM model is widely regarded as the most successful. It adopts the cosmological constant $\Lambda$ as DE and cold dark matter (CDM), and has demonstrated good agreement with most of the observational data. However, it faces several theoretical challenges, including the "fine-tuning" and the "cosmic coincidence" problems [7]. Furthermore, with the advent of increasingly precise cosmological data, a significant tension involving the $\Lambda$CDM has emerged, commonly referred to as the Hubble tension [8–17]. This tension arises from the $5\sigma$ discrepancy between two independent estimates of the Hubble constant: the value inferred from the Planck cosmic microwave background (CMB) measurements based on the $\Lambda$CDM model, $H_0 = 67.4 \pm 0.50$ km s$^{-1}$ Mpc$^{-1}$ [18], and the value directly measured by the Hubble Space Telescope (HST) using Cepheid variables in the host galaxies of 42 type Ia supernova (SNIa), $H_0 = 73.04 \pm 1.04$ km s$^{-1}$ Mpc$^{-1}$ [19].

In response to these challenges, various dynamical dark energy models have been proposed to address the limitations of the $\Lambda$CDM model, particularly those arising from the cosmological constant as the source of DE. These include scalar-field models such as quintessence [20,21], phantom [22,23], quintom [24–26], and k-essence [27,28], interacting dark energy models [29,30], metastable dark energy models [31], running vacuum models [32,33], early dark energy

[a] e-mail: xub@ahstu.edu.cn (corresponding author)
[b] e-mail: ktzhang@ahnu.edu.cn (corresponding author)

Published online: 15 September 2025

scenarios [34], unified dark sector models such as the generalized Chaplygin gas [35,36], and nonlocal effective fluid models [37,38], as well as phenomenological parameterizations of dynamical dark energy [39–42]. For a broader perspective on dynamical alternatives to the standard ΛCDM paradigm, we refer the reader to Refs. [43–45]. Among these, the holographic dark energy (HDE) model inspired by the holographic principle [46], is a successful candidate for DE and has been widely studied. Initially, Cohen et al. [47] proposed a relationship between the ultraviolet (UV) cut-off at a short distance and the infrared (IR) cut-off at a large distance, through which the DE viewed as the vacuum energy can be represented with the cut-off. However, the original HDE model, which took the Hubble scale as IR cut-off, struggled to explain the current cosmic accelerated expansion [48]. To address this issue, Li et al. proposed a new HDE model that adopts the future event horizon as the IR cut-off [49]. This model not only successfully accounts for the current cosmic accelerated expansion, but also completely resolves the causality problem and circular logic problem inherent in the original HDE model. The HDE has become a highly competitive candidate for DE, attracting notable attention in recent years [50–64]. Nevertheless, the subsequent observational constraints on the HDE model indicate that the equation of state parameter of DE tends to approach values less than $-1$ in the future, suggesting that the universe could eventually face the fate of the Big Rip [65–71].

Since the HDE model encounters the Big Rip singularity, which threatens its theoretical foundation, a widely adopted approach is to introduce an interaction between HDE and matter, referred to as the interacting holographic dark energy (IHDE) model [72–81]. Li et al. [82] found in this model the interaction term often brings about an attractor solution to the evolution equation, where the effective equations of state for DE and matter tend to be the same in the far future. Furthermore, according to the works [83,84], the IHDE model can significantly alleviate the coincidence problem. The IHDE model has been extensively tested using various observations, including baryon acoustic oscillations (BAO), SNIa, the cosmic microwave background (CMB), and observational Hubble parameter data (OHD), with well support, as demonstrated by Refs. [85–87].

Most recently, the Dark Energy Spectroscopic Instrument (DESI) collaboration released the baryon acoustic oscillation (BAO) measurements from its second data release (DR2), covering the first three years of operation [90–93]. With over 30 million spectroscopic redshifts of galaxies and quasars, along with Ly$\alpha$ forest spectra from more than 820,000 quasars, DESI DR2 represents the largest spectroscopic galaxy sample to date. By combining this BAO data with the Dark Energy Survey 5-Year SNIa (DES-SN5Y) datasets [94] and the Planck 2018 CMB data within the framework of the Chevallier–Polarski–Linder (CPL) parameterization, the DESI collaboration reported a deviation of up to $4.2\sigma$ from the ΛCDM model [90], offering stronger evidence for a dynamical dark energy scenario than that obtained from its first data release (DR1) [95–97]. DESI BAO measurements, as an essential tool for exploring the potential dynamical properties of DE, have been widely used in cosmological studies [98–112]. In the past year, Li et al. [113] utilized DESI DR1 BAO, CMB, and SNIa data to investigate the cosmological implications of the HDE model and the IHDE model with an interaction form of $Q \propto H\rho_{\rm de}$, and found that both the HDE and IHDE models are significantly less favored compared to the ΛCDM model. In another study, Li and Wang [114] used DESI DR1 BAO to conduct a comprehensive numerical analysis of four categories of HDE models: those with alternative characteristic length scales, extended Hubble scales, dark sector interactions, and modified black hole entropy. Notably, their results show that the IHDE model with the interaction form $Q \propto H\,(\rho_{\rm dm} + \rho_{\rm de})$ is disfavored by the BAO+CMB+SNIa data. Building on these studies, this paper focuses on revisiting the viability of IHDE models with ten representative interaction forms [86,87], which previously showed good agreement with the observational data available at the time. The analysis utilizes the latest datasets, including DESI DR2 BAO, DES-SN5Y, Planck 2018 CMB, OHD, and the local measurement of Hubble constant given by Riess et al. Through a comprehensive numerical analysis, we aim to explore the parameter constraints of the HDE and IHDE models based on the current observational data, and identify the most viable models based on the Akaike Information Criterion (AIC) and Bayesian Information Criterion (BIC).

The structure of this paper is organized as follows: Sect. 2 introduces the IHDE models with ten interaction forms in a spatially flat universe. Section 3 describes the datasets and methodology used in our analysis. In Sect. 4, we present the constraint results and the analysis. Finally, Sect.5 summarizes our conclusions.

## 2 The IHDE model

According to the holographic principle of quantum gravity theory, when gravity is considered, the quantum zero-point energy of a system with size $L$ should not exceed the mass of a black hole with the equivalent size [47]. Extending this concept to the entire universe, the vacuum energy associated with the holographic principle is interpreted as the DE, commonly referred to as HDE, with its density expressed as

$$\rho_{\rm de} = 3c^2 M_{\rm pl}^2 L^{-2}, \tag{1}$$

where $c$ is a dimensionless constant, $M_{\rm pl} = \frac{1}{\sqrt{8\pi G}}$ is the reduced Planck mass, and $L$ denotes the IR cut-off size. In this paper, we adopt the future event horizon of the universe as the IR cut-off $L$, as defined in [49]:

$$L = a(t)\int_t^\infty \frac{dt'}{a(t')} = a\int_a^\infty \frac{da'}{Ha(t')^2}, \tag{2}$$

where $a(t)$ is the scale factor, and $H = \frac{\dot{a}}{a}$ is the Hubble parameter, with the dot denoting the derivative with respect to the cosmic time $t$.

For a spatially-flat universe, the Friedmann equation can be expressed as

$$3M_{\rm pl}^2H^2 = \rho_{\rm dm} + \rho_{\rm b} + \rho_{\rm r} + \rho_{\rm de}, \tag{3}$$

where $\rho_{\rm dm}$, $\rho_{\rm b}$, $\rho_{\rm r}$ and $\rho_{\rm de}$ represent energy density of dark matter (DM), baryon, radiation, and DE, respectively. It is convenient to express these components in terms of their fractional energy densities, defined as

$$\Omega_{\rm dm} = \frac{\rho_{\rm dm}}{\rho_{\rm c}},\quad \Omega_{\rm b} = \frac{\rho_{\rm b}}{\rho_{\rm c}},\quad \Omega_{\rm r} = \frac{\rho_{\rm r}}{\rho_{\rm c}},\quad \Omega_{\rm de} = \frac{\rho_{\rm de}}{\rho_{\rm c}}, \tag{4}$$

where $\rho_{\rm c} = 3M_{\rm pl}^2H^2$ is the critical density of the universe. The fractional energy density of matter is given by $\Omega_{\rm m} = \Omega_{\rm dm} + \Omega_{\rm b}$, and it follows that

$$\Omega_{\rm m} + \Omega_{\rm r} + \Omega_{\rm de} = 1. \tag{5}$$

In addition, the relation between the present-day fractional energy densities of radiation and matter is given by $\Omega_{\rm r0} = \Omega_{\rm m0}/\left(1+z_{\rm eq}\right)$, where $z_{\rm eq} = 2.5\times10^4\Omega_{\rm m0}h^2\left(T_{\rm cmb}/2.7{\rm K}\right)^{-4}$, with $T_{\rm cmb} = 2.7255{\rm K}$.

In this work, the interactions between the DM and HDE are considered. The energy conservation equations can be written as

$$\dot{\rho}_{\rm dm} + 3H\rho_{\rm dm} = Q, \tag{6}$$

$$\dot{\rho}_{\rm de} + 3H\left(\rho_{\rm de} + P_{\rm de}\right) = -Q, \tag{7}$$

where $Q$ is the interaction term describing the transfer rate between dark sectors in the IHDE model. The functional form of $Q$ is not uniquely defined and can take various phenomenological expressions. Specifically, when $Q = 0$, the model reduces to the standard HDE scenario. Building on previous studies [85–87], we will impose new observational constraints on the IHDE models with ten representative interaction forms, as summarized in Table 1. These interaction forms are categorized into two groups: one involving the Hubble parameter $H$, and the other involving its present-day value $H_0$. It is worth noting that in the interaction term, the coupling parameter $\beta$ governs the direction and intensity of the energy flow between the dark components. A positive $\beta$ implies that DE decays into DM. Conversely, a negative $\beta$ corresponds to a transfer from DM to DE.

**Table 1** Summary of the two categories of interaction forms considered in this work

| IHDE | Q with H | IHDE | Q with $H_0$ |
|---|---|---|---|
| I-A | $3\beta H\rho_{\rm de}$ | I-B | $3\beta H_0\rho_{\rm de}$ |
| II-A | $3\beta H\rho_{\rm dm}$ | II-B | $3\beta H_0\rho_{\rm dm}$ |
| III-A | $3\beta H\left(\rho_{\rm dm}+\rho_{\rm de}\right)$ | III-B | $3\beta H_0\left(\rho_{\rm dm}+\rho_{\rm de}\right)$ |
| IV-A | $3\beta H\sqrt{\rho_{\rm dm}\rho_{\rm de}}$ | IV-B | $3\beta H_0\sqrt{\rho_{\rm dm}\rho_{\rm de}}$ |
| V-A | $3\beta H\frac{\rho_{\rm dm}\rho_{\rm de}}{\rho_{\rm dm}+\rho_{\rm de}}$ | V-B | $3\beta H_0\frac{\rho_{\rm dm}\rho_{\rm de}}{\rho_{\rm dm}+\rho_{\rm de}}$ |

Combining Eqs. (1–7) and performing some calculations [85], the dynamical evolution equations of IHDE are obtained as:

$$\frac{1}{E}\frac{{\rm d}E}{{\rm d}z} = -\frac{\Omega_{\rm de}}{1+z}\left(\frac{1}{c}\sqrt{\Omega_{\rm de}} + \frac{1}{2} + \frac{\Omega_{\rm I}-3-\Omega_{\rm r}}{2\Omega_{\rm de}}\right), \tag{8}$$

$$\frac{{\rm d}\Omega_{\rm de}}{{\rm d}z} = -\frac{2\left(1-\Omega_{\rm de}\right)\Omega_{\rm de}}{1+z}\left(\frac{1}{c}\sqrt{\Omega_{\rm de}} + \frac{1}{2} - \frac{\Omega_{\rm I}-\Omega_{\rm r}}{2\left(1-\Omega_{\rm de}\right)}\right), \tag{9}$$

where $E(z) = H(z)/H_0$, $\Omega_{\rm I} = Q/(3M_{\rm pl}^2H^3)$.

## 3 Data and methodology

### 3.1 Observational data

In this paper, we aim to revisit the viability of IHDE models using the latest observational data, which include BAO, SNIa, CMB, OHD, and $H_0$ measurements, as detailed below.

- *BAO* BAO describes the clustering of baryonic matter at specific length scales, resulting from the propagation of acoustic waves in the early universe. These oscillations imprint characteristic scales that act as a cosmic standard ruler, enabling precise distance measurements in cosmology. Most recently, the DESI Collaboration released its DR2 BAO measurements from the first three years of operation [90]. The dataset includes four classes of extragalactic targets [90,91]: bright galaxy survey (BGS), and quasar (QSO), luminous red galaxy (LRG), emission line galaxies (ELG), and Lyman-$\alpha$ quasars (Ly$\alpha$ QSO). The BAO measurements [115] correspond to three types of distances: $D_{\rm M}(z)/r_{\rm d}$, $D_{\rm V}(z)/r_{\rm d}$, and $D_{\rm H}(z)/r_{\rm d}$. Here, $D_{\rm M}$ is the transverse comoving distance, $D_{\rm V}$ is the angle-averaged distance, $D_{\rm H}$ is the Hubble distance. Additionally, $r_{\rm d}$ denotes the sound horizon at the baryon drag

epoch $z_d$ determined by the fitting formula for $z_d$ given in Ref. [116], and $r_d$ can be expressed as

$$r_d = \int_{z_d}^{\infty} \frac{c_s(z')}{H(z')} dz', \tag{10}$$

where $c_s(z)$ is the sound speed in the photon-baryon fluid, given by

$$c_s(z) = \frac{c}{\sqrt{3\left(1+\frac{3\rho_{b0}}{4\rho_{\gamma 0}}\right)}}, \tag{11}$$

with $\rho_{b0}$ and $\rho_{\gamma 0}$ represent the present-day energy densities of baryons and photons, respectively. Moreover, we adopt the following relation:

$$3\rho_{b0}/(4\rho_{\gamma 0}) = 31500\Omega_{b0}h^2 \left(T_{\rm cmb}/2.7{\rm K}\right)^{-4}. \tag{12}$$

It is worth emphasizing that the result obtained by directly calculating $r_d$ using the above formula differs from the values derived by solving the Boltzmann equation with the CAMB code [117], and does not agree with the calibration approximation results used by the BOSS [118] and DESI [90] collaborations. Therefore, to achieve more accurate results, a correction factor of approximately 0.9732 should be applied by the above formula [120], and the revised $r_d$ is consistent with their results. In this work, we adopt the corrected formula.
The $\chi^2$ function of BAO data can be written as:

$$\begin{aligned}\chi^2_{\rm BAO} = &\chi^2_{\rm BGS} + \chi^2_{\rm LRG1} + \chi^2_{\rm LRG2} + \chi^2_{\rm LRG3+ELG1} \\ &+\chi^2_{\rm ELG2} + \chi^2_{\rm QSO} + \chi^2_{\rm Ly\alpha QSO},\end{aligned} \tag{13}$$

where the $\chi^2$ for the QSO, LRG1, LRG2, ELG2, Ly$\alpha$QSO, and LRG3+ELG1 data are given in the form of $\chi^2_i = (\eta^{th}_i - \eta^{obs}_i)^T \cdot Cov_i^{-1} \cdot (\eta^{th}_i - \eta^{obs}_i)$. The vector $\eta^{obs}_i$ represents the observational data for the $i$th dataset, $\eta^{th}_i$ is the prediction for these vectors in a given cosmological model, and $Cov_i$ is the covariance matrix of the respective dataset.

- *SNIa*
As standard candles, SNIa are widely used to probe the expansion rate and large-scale properties of the Universe. In our analysis, we use the latest DES-SN5Y sample, which includes 1,635 SNIa over the redshift range $0.1 < z < 1.3$, complemented by a high-quality external low-redshift sample of 194 SNIa spanning $0.025 < z < 0.1$ [94].
The observed distance modulus $\mu_{\rm obs}$ is defined as

$$\mu_{\rm obs} = m^*_{\rm B} + \alpha X_1 - \beta C - M_{\rm B}\,, \tag{14}$$

where, $m^*_{\rm B}$ is the observed peak magnitude in the rest-frame B band, $X_1$ represents the time stretching of the light curve, $C$ denotes the SNIa color at maximum brightness, $M_B$ is the absolute magnitude, and $\alpha$, $\beta$ are two nuisance parameters.
The theoretical value of the distance modulus can be derived as

$$\mu_{\rm th}(z) = 5\log(d_{\rm L}) + \mu_0\,, \tag{15}$$

where $d_L(z) = (1+z)\int_0^{z'} \frac{dz'}{E(z')}$, $\mu_0 = 42.38 - 5\log h$ with $h = H_0/100$ km s$^{-1}$Mpc$^{-1}$. Thus, the $\chi^2$ function for the DES-SN5Y data can be expressed as

$$\chi^2_{\rm SNIa} = \Delta\mu^T \cdot (C_{\rm SNIa})^{-1} \cdot \Delta\mu, \tag{16}$$

where $\Delta\mu = \Delta m - M_B - \mu_0$, and $C_{\rm SNIa}$ is the covariance matrix of SNIa. Following the method proposed in Conley et al. [122], $M_B + \mu_0$ is analytically marginalized using a flat prior. Then the $\chi^2$ function can be rewritten as

$$\chi^2_{SNIa} = a + \ln\frac{b}{2\pi} - \frac{f^2}{b}, \tag{17}$$

where $a \equiv (\Delta m)^T \cdot (C_{\rm SNIa})^{-1} \cdot \Delta m$, $b \equiv \mathbf{1}^T \cdot (C_{\rm SNIa})^{-1} \cdot \mathbf{1}$, and $f \equiv (\Delta m)^T \cdot (C_{\rm SNIa})^{-1} \cdot \mathbf{1}$.

- *CMB*
The CMB radiation encodes crucial information about the evolution of the early universe and large-scale structure formation. Typically, the standard analysis of full CMB data involves comparing the observed temperature power spectrum with theoretical predictions from a specific cosmological model, which requires complete and accurate modeling of linear perturbations. While this approach works effectively for $\Lambda$CDM and its minimal extensions, it becomes non-trivial and computationally challenging for non-minimal models, particularly in scenarios involving dynamical dark energy [119]. In this work, we focuses on the background-level analysis of IHDE model. To facilitate efficient computation, we adopt the distance prior compressed from the Planck 2018 release [120]. This prior provides precise constraints on the cosmic expansion and serves as a reliable substitute for the full dataset published by Planck in 2018 [121]. It is characterized by two parameters: the acoustic scale $l_{\rm A}$, and the shift parameter $R$, defined as follows:

$$R = (1+z_*)\sqrt{\Omega_{\rm m,0}H_0^2}D_{\rm A}(z_*)/c_0, \tag{18}$$

$$l_{\rm A} = (1+z_*)\,\pi\, D_{\rm A(z_*)}/r_{\rm s}(z_*)\,, \tag{19}$$

where $D_A$ is the angular diameter distance, and $r_s(z_*)$ represents the comoving sound horizon at the photon decoupling epoch corresponding to redshift $z_*$, which can be estimated using an approximate formula provided in Ref. [123]. The constant $c_0$ denotes the speed of light. The $\chi^2$ function for the distance priors can be expressed by

$$\chi^2_{\rm CMB} = \sum_{i,j} \left(x_i^{\rm obs} - x_i^{\rm th}\right) \left(C^{-1}_{\rm CMB}\right)_{ij} \left(x_j^{\rm obs} - x_j^{\rm th}\right), \tag{20}$$

here $x = \{R(z_*), l_A(z_*), \omega_{b0}\}$, and $\omega_{b0} = \Omega_{b0}h^2$ with $\Omega_{b0}$ representing the current fractional energy density of baryons. The superscript obs denoting the mean values obtained from CMB observations, and th representing the theoretical values predicted by cosmological models. The term $C_{\rm CMB}$ refers to the covariance matrix of distance priors.

- *OHD*
  The OHD dataset used in this study consists of 32 $H(z)$ data points obtained from the cosmic chronometers (CC) method, as listed in the Ref. [124], covering a redshift range of $0.07 \leq z \leq 1.965$. These measurements are derived from the differential ages of passively evolving galaxies at various redshifts, which can be described by the following formula [125]:

$$H(z) \simeq -\frac{1}{1+z}\frac{\triangle z}{\triangle t}. \tag{21}$$

  The $\chi^2$ function for the OHD data can be written as

$$\chi^2_{OHD} = \Delta H^T \cdot (C_{\rm OHD})^{-1} \cdot \Delta H\ , \tag{22}$$

  where $\Delta H = H_{th} - H_{obs}$ represents the difference between the theoretical and observed Hubble parameters, and $C_{\rm OHD}$ denotes the full covariance matrix, which contains both statistical and systematic errors [126].

- *The local measurement of $H_0$*
  We adopt the latest Hubble constant measurements from Riess et al. [19], with the observed value $H_0^{\rm obs} = 73.04 \pm 1.04\ {\rm km\ s^{-1}\ Mpc^{-1}}$. This result is derived using Cepheid variables in the host galaxies of 42 Type Ia supernovae, observed with the Hubble Space Telescope, to precisely calibrate the Hubble constant.
  The $\chi^2$ function for the Hubble constant is expressed as

$$\chi^2_{H_0} = \left(\frac{H_0^{\rm th} - 73.04}{1.04}\right)^2, \tag{23}$$

  where $H_0^{\rm th}$ is the theoretical predicted value in the cosmological models.

To fit the IHDE models, we carry out the Markov Chain Monte Carlo (MCMC) analysis using the CosmoMC package [88]. Convergence of the MCMC chains is set to $R - 1 < 0.01$, based on the Gelman–Rubin statistic [89]. The IHDE model involves five free parameters: $H_0$, $\Omega_m$, $\Omega_b h^2$, $c$, and $\beta$, and we impose uniform priors adopted over the following ranges: $H_0 \in [40, 100]\ {\rm km\ s^{-1}\ Mpc^{-1}}$, $\Omega_m \in [0.1, 0.6]$, $\Omega_b h^2 \in [0.005, 0.1]$, $c \in [0, 3]$, and $\beta \in [-1, 1]$.

### 3.2 Model comparison methods

To further determine the optimal model among various candidates, it is essential to evaluate how well each model fits the data using model comparison methods.

- *Information criterion*
  The most commonly used metrics are the Akaike information criterion (AIC) [127] and the Bayesian information criterion (BIC) [128], which are defined as follows

$$\mathrm{AIC} = -2\ln L_{\max} + 2n = \chi^2_{\min} + 2n, \tag{24}$$
$$\mathrm{BIC} = -2\ln L_{\max} + n\ln N = \chi^2_{\min} + n\ln N, \tag{25}$$

  where $\chi^2_{\min}$ is the sum of the minimum chi-square values over all datasets, $n$ denotes the number of model parameters, and $N$ represents the total number of data points. In practice, model selection is based on comparing the differences in AIC and BIC values between competing models, given by:

$$\Delta\mathrm{AIC} = \Delta\chi^2_{\min} + 2\Delta n, \tag{26}$$
$$\Delta\mathrm{BIC} = \Delta\chi^2_{\min} + \Delta n\ln N. \tag{27}$$

  In general, the model with $\Delta\mathrm{AIC} \geq 5$ or $\Delta\mathrm{AIC} \geq 10$ is considered to be strongly or very strongly disfavored compared to the preferred model, respectively. Similarly, for BIC, the conditions $\Delta\mathrm{BIC} \geq 2$ or $\Delta\mathrm{BIC} \geq 6$ indicates the same level of preference.
- *Bayes factor*
  The statistical measures discussed above do not explicitly incorporate the prior range of the analysis. Since the inclusion of explicit priors can substantially impact

**Table 2** Revised Jeffreys scale quantifying the observational viability of any model $\mathcal{M}_i$ compared with some reference model $\mathcal{M}_j$

| $\ln B_{ij}$ | Strength of evidence for model $\mathcal{M}_i$ |
|---|---|
| $0 < \lvert\ln B_{ij}\rvert < 1$ | Weak |
| $1 < \lvert\ln B_{ij}\rvert < 3$ | Definite/positive |
| $3 < \lvert\ln B_{ij}\rvert < 5$ | Strong |
| $\lvert\ln B_{ij}\rvert > 5$ | Very strong |

both the optimal values and the statistical preference of the model, we also employ the Bayesian evidence approach, which accounts for the entire posterior distribution. Bayesian evidence provides a statistical way to evaluate the statistical preference for one model over another by computing the Bayes factor. For a given model $\mathcal{M}$ with parameter space $\theta$ and specific observational data $d$, the Bayesian evidence $E$ is defined as

$$E = p(d|\mathcal{M}) = \int p(d|\theta, \mathcal{M})\pi(\theta|\mathcal{M})d\theta, \tag{28}$$

where $\pi(\theta|\mathcal{M})$ is the prior of $\theta$ in model $\mathcal{M}$, and $p(d|\theta, \mathcal{M})$ is the likelihood. Then, for the two models $\mathcal{M}_i$ and $\mathcal{M}_j$, combing the Bayes theorem, the posterior probability is

$$\frac{p(\mathcal{M}_i|d)}{p(\mathcal{M}_j|d)} = \frac{p(d|\mathcal{M}_i)}{p(d|\mathcal{M}_j)}\frac{\pi(\mathcal{M}_i)}{\pi(\mathcal{M}_j)}. \tag{29}$$

The ratio between posterior probabilities leads to the definition of the Bayes factor $B_{ij}$, which is written in a logarithmic scale as

$$\ln B_{ij} = \ln \frac{p(d|\mathcal{M}_i)}{p(d|\mathcal{M}_j)} = \ln p(d|\mathcal{M}_i) - \ln p(d|\mathcal{M}_j). \tag{30}$$

Then, one can determine the strength of the preference for one of the competing models over the other by means of the Jeffreys scale listed in Table 2 [129,130].

We employ the nested sampling plugin PolyChord [131, 132] within the CosmoMC framework, which enables efficient computation of the Bayesian model evidence.

## 4 Results and discussion

We use the dataset BAO+SNIa+CMB+OHD+$H_0$ to investigate the HDE and the IHDE models. The constrained results, which include the mean values and 68.3% confidence level (CL) for the cosmological and model parameters ($H_0$, $\Omega_{m,0}$, $c$, $\Omega_b h^2$, $\beta$ ), are summarized in Table 3, comparing the ten IHDE models with the ΛCDM and HDE models. The likelihood distributions of these parameters are illustrated in Figs. 1, 2, 3, 4, 5 and 6. Additionally, we apply three model selection methods to compare these models, with the corresponding ΔAIC, ΔBIC and $\ln B_{ij}$ values presented in Table 4.

We first focus on the model parameter $c$, which plays a crucial role in governing the evolution of DE. As shown in Table 3, $c$ remains less than 1 in all HDE and IHDE models considered, suggesting DE exhibits phantom-like behavior in the future, potentially leading to the big rip problem. Compared to the HDE model, the IHDE models yield higher central values of $c$, with a reduced statistical deviation from $c = 1$, which may potentially alleviate the Big Rip problem. It is noteworthy that the IHDE I-B and IHDE V-B models have the highest central values of $c$, which are $0.817^{+0.029}_{-0.035}$ and $0.806^{+0.029}_{-0.033}$ at one standard deviation, respectively, while the IHDE II-A model has the lowest central value, $0.749^{+0.023}_{-0.027}$ at one standard deviation. Our constraints are consistent with those obtained by Feng et al. [86] and Li et al. [87], based on Planck 2015 CMB data, the Joint Light-Curve Analysis (JLA) of SNIa, baryon acoustic oscillation data, and local measurements of the Hubble constant.

Second, we analyze the model parameter $\beta$, which governs the energy exchange between DE and DM. As shown in Table 3, $\beta$ is positive in all IHDE models, at a CL exceeding $7\sigma$, providing strong evidence for the decay of DE into DM.

**Table 3** Summary of constraints on the model parameters at the 68% CL

| Parameter | $H_0$ | $\Omega_{m,0}$ | $\Omega_{b,0}h^2$ | $c$ | $\beta$ |
|---|---|---|---|---|---|
| ΛCDM | $68.82 \pm 0.28$ | $0.2980 \pm 0.0035$ | $0.02260 \pm 0.00013$ | – | – |
| HDE | $68.61 \pm 0.48$ | $0.2911 \pm 0.0042$ | $0.02291 \pm 0.00013$ | $0.711 \pm 0.021$ | – |
| IHDE I-A | $68.91 \pm 0.51$ | $0.3038 \pm 0.0049$ | $0.02237 \pm 0.00015$ | $0.804^{+0.028}_{-0.033}$ | $0.0183 \pm 0.0024$ |
| IHDE I-B | $68.92 \pm 0.50$ | $0.3039 \pm 0.0048$ | $0.02237 \pm 0.00015$ | $0.817^{+0.029}_{-0.035}$ | $0.0244 \pm 0.0033$ |
| IHDE II-A | $68.86 \pm 0.51$ | $0.3024 \pm 0.0047$ | $0.02243 \pm 0.00015$ | $0.749^{+0.023}_{-0.027}$ | $0.00577 \pm 0.00079$ |
| IHDE II-B | $68.92 \pm 0.50$ | $0.3036 \pm 0.0047$ | $0.02237 \pm 0.00015$ | $0.784^{+0.027}_{-0.031}$ | $0.0201 \pm 0.0026$ |
| IHDE III-A | $68.87 \pm 0.50$ | $0.3027 \pm 0.0046$ | $0.02242 \pm 0.00015$ | $0.763 \pm 0.026$ | $0.00443 \pm 0.00060$ |
| IHDE III-B | $68.92 \pm 0.52$ | $0.3039 \pm 0.0048$ | $0.02237 \pm 0.00015$ | $0.798^{+0.029}_{-0.034}$ | $0.0111 \pm 0.0015$ |
| IHDE IV-A | $68.95 \pm 0.50$ | $0.3031 \pm 0.0047$ | $0.02238 \pm 0.00015$ | $0.779^{+0.026}_{-0.030}$ | $0.0143 \pm 0.0018$ |
| IHDE IV-B | $68.92 \pm 0.51$ | $0.3038 \pm 0.0047$ | $0.02237 \pm 0.00015$ | $0.803^{+0.028}_{-0.033}$ | $0.0249 \pm 0.0033$ |
| IHDE V-A | $68.94 \pm 0.50$ | $0.3035 \pm 0.0046$ | $0.02237 \pm 0.00015$ | $0.789^{+0.027}_{-0.031}$ | $0.0358 \pm 0.0044$ |
| IHDE V-B | $68.93 \pm 0.51$ | $0.3038 \pm 0.0047$ | $0.02237 \pm 0.00015$ | $0.806^{+0.029}_{-0.033}$ | $0.0544 \pm 0.0070$ |

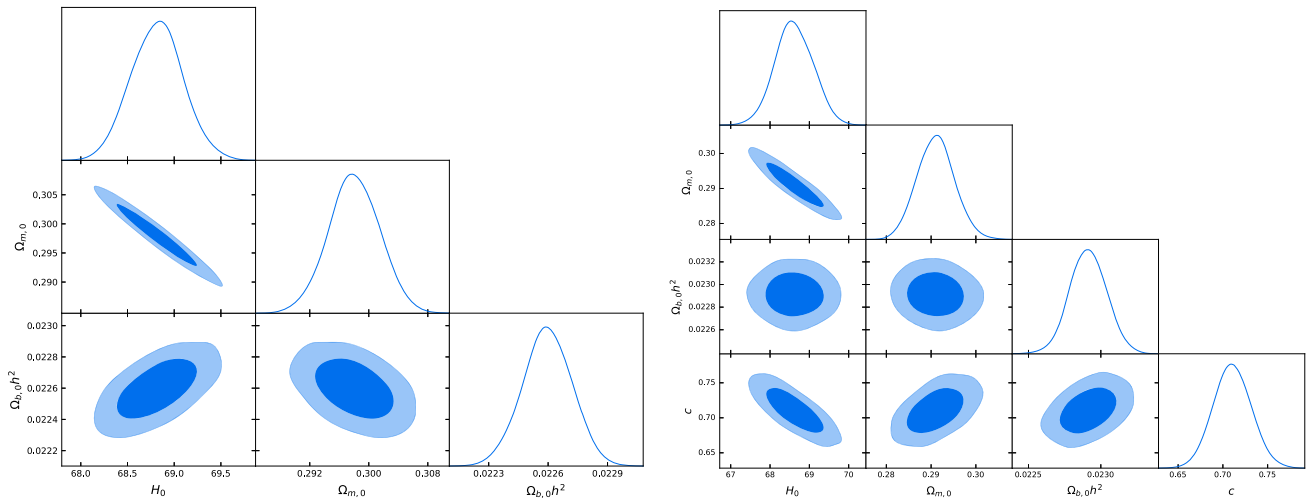


**Fig. 1** The contour plots (68.3% and 95.4% CLs) and marginalized probability distributions for the parameters $H_0$, $\Omega_{\mathrm{m},0}$ and $c$ in the ΛCDM (left panel) and HDE (right panel) models without interaction

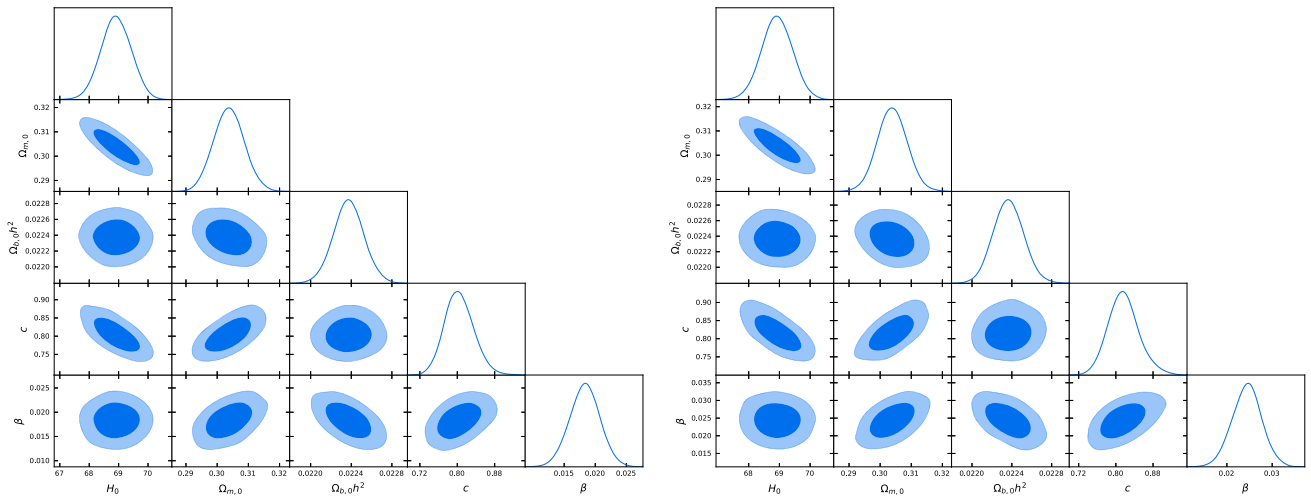


**Fig. 2** The contour plots (68.3% and 95.4% CLs) and marginalized probability distributions for the parameters $H_0$, $\Omega_{\mathrm{m},0}$, $c$, $\Omega_{\mathrm{b}}h^2$ and $\beta$ in the IHDE I-A (left panel) and IHDE I-B (right panel) models

The IHDE V-A model exhibits the strongest statistical evidence for a positive $\beta$, reaching the $8.1\sigma$ CL. This result is consistent with previous studies [79,85–87]. From Figs. 2, 3, 4, 5, and 6, we observe a positive correlation between $\beta$ and $c$. As $\beta$ increases, $c$ approaches 1, indicating that the interaction term driving DE decay into DM may help alleviate the Big Rip problem.

Third, we examine the constraints on the cosmological parameters $\Omega_{m,0}$, $\Omega_{b,0}$, and $H_0$. As shown in Table 3, the IHDE models remain consistent with the ΛCDM models within $1.2\sigma$ for these parameters. For $H_0$, all IHDE models exhibit slightly higher central values compared to the ΛCDM model, whereas the HDE model shows a slightly lower central value. Both the HDE model and all IHDE models remain consistent with the Planck 2018 results [18] within the $2.2\sigma$ CL. However, they exhibit a significant tension with the local measurement of the Hubble constant by Riess et al. [10], with discrepancies exceeding the $3.5\sigma$ level. These findings are in line with previous studies [113,114], where analyses using DESI BAO+SNIa+CMB data, also found that the IHDE models considered are in better agreement with the Planck 2018 results while maintaining a substantial tension with the local $H_0$ determination. Furthermore, from Figs. 1, 2, 3, 4, 5 and 6, we observe a negative correlation between $H_0$ and parameter $c$, suggesting that a smaller value of $c$ can lead to a larger $H_0$, thereby alleviating the Hubble tension while worsening the Big Rip problem.

Finally, we evaluate model selection based on the AIC, BIC, and Bayes factor to determine the best fit to the observational data. As shown in Table 4, all the HDE and IHDE models considered have ΔAIC and ΔBIC values greater than zero, indicating that the ΛCDM model remains the most

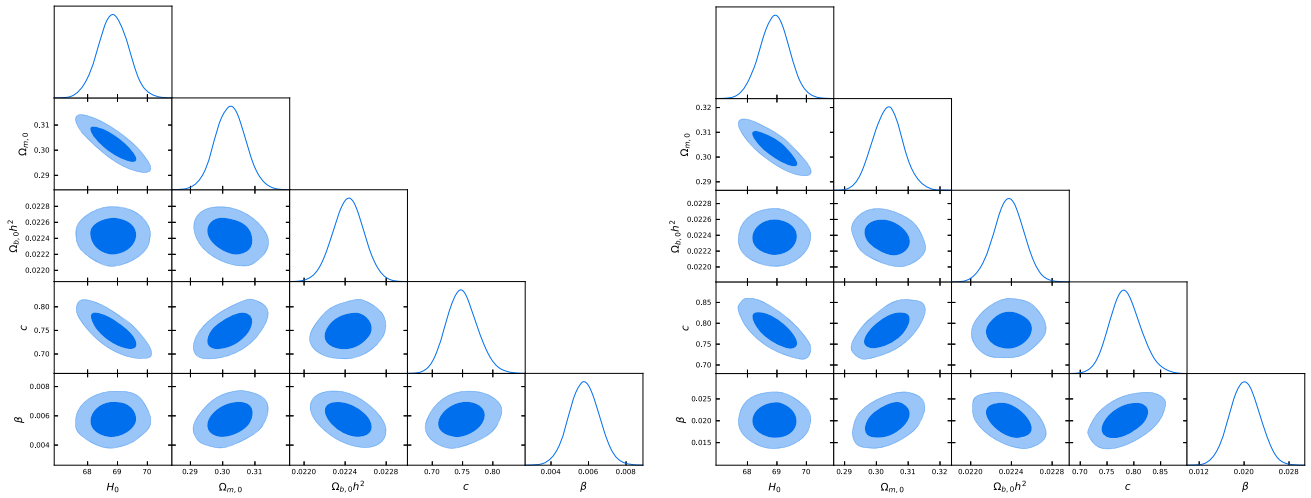


**Fig. 3** The contour plots (68.3% and 95.4% CLs) and marginalized probability distributions for the parameters $H_0$, $\Omega_{\mathrm{m},0}$, $c$, $\Omega_{\mathrm{b}}h^2$ and $\beta$ in the IHDE II-A (left panel) and IHDE II-B (right panel) models

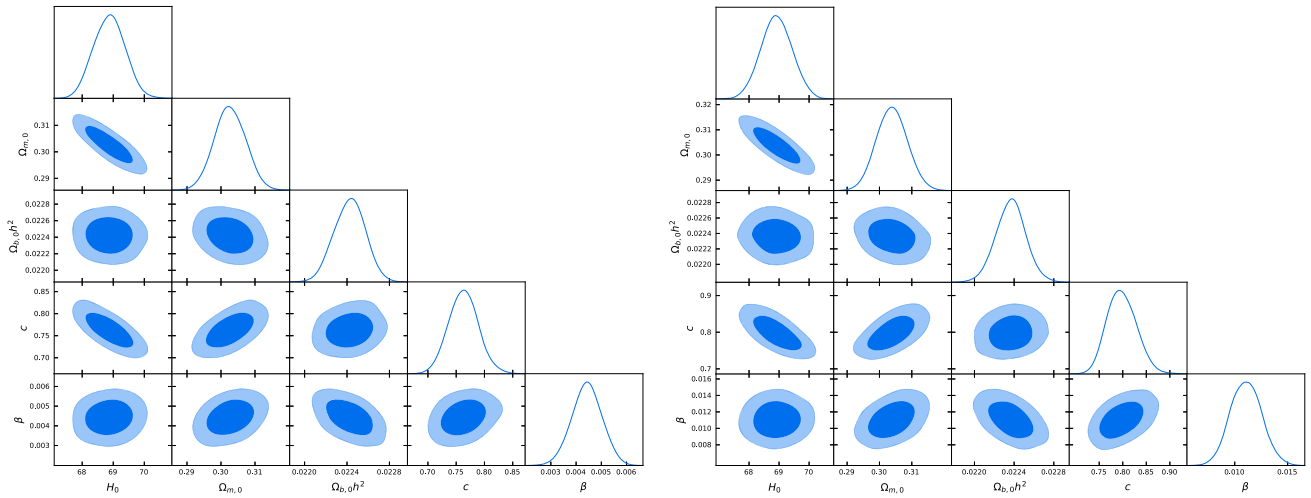


**Fig. 4** The contour plots (68.3% and 95.4% CLs) and marginalized probability distributions for the parameters $H_0$, $\Omega_{\mathrm{m},0}$, $c$, $\Omega_{\mathrm{b}}h^2$ and $\beta$ in the IHDE III-A (left panel) and IHDE III-B (right panel ) models

favored by the current data. Moreover, it is evident that the current data clearly rule out the HDE model. But compared to the HDE model, the IHDE models show improved agreement with the data. Among all the IHDE models, the IHDE I-B($Q = 3\beta H_0 \rho_{\mathrm{de}}$), and IHDE V-B($Q = 3\beta H_0 \frac{\rho_{\mathrm{dm}}\rho_{\mathrm{de}}}{\rho_{\mathrm{dm}}+\rho_{\mathrm{de}}}$) models yield the lowest $\Delta$AIC, $\Delta$BIC and ln $B_{ij}$ value, indicating that they are the two most favored IHDE models based on the observational data. These findings are generally consistent with previous studies. [86,87]. Additionally, the $\Delta$AIC, $\Delta$BIC and ln $B_{ij}$ values for the majority of IHDE models are similar, indicating that the current data do not strongly differentiate between them in most cases. This highlights the need for more precise data to further assess the viability of these models in the future.

## 5 Conclusions

In this study, we revisit the viability of IHDE models by investigating ten representative interaction forms. Our analysis is based on the latest observational datasets, including the DESI DR2 BAO data, the DES-SN5Y supernova sample, the OHD, the Planck 2018 CMB data, and the local $H_0$ measurement given by Riess et al. Using the CosmoMC package, we perform an MCMC analysis to derive constraints on cosmological and model parameters. Based on these constraints, we systematically compare the IHDE models with the HDE and $\Lambda$CDM models. Finally, we apply AIC, BIC, and Bayes factor to evaluate the IHDE models and identify those most favored by the observational data.

Our joint constraints indicate that the IHDE models are consistent with the $\Lambda$CDM models within the $1.2\sigma$ CL for

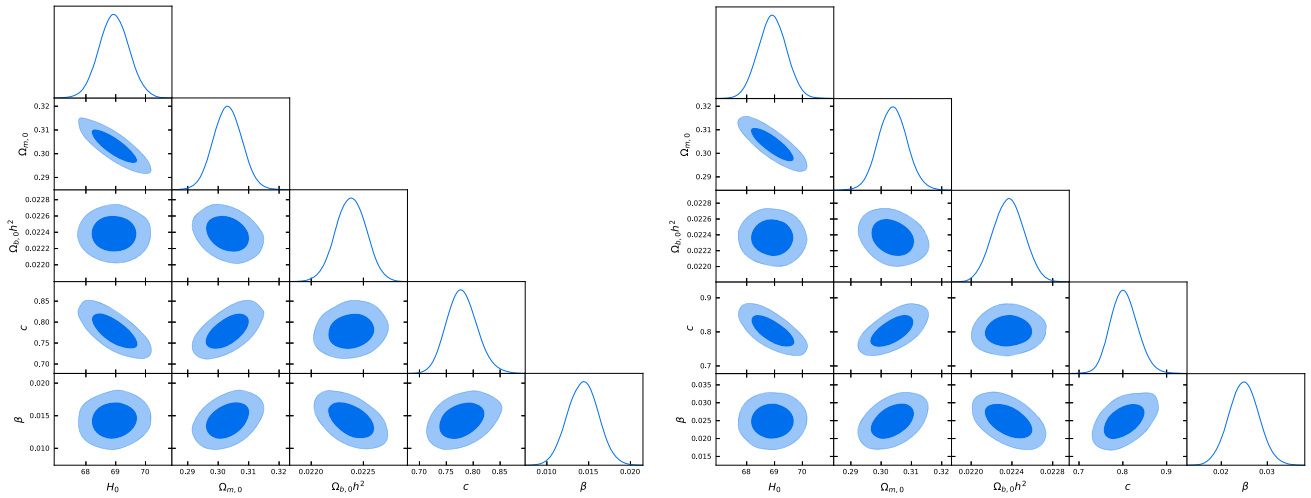


**Fig. 5** The contour plots (68.3% and 95.4% CLs) and marginalized probability distributions for the parameters $H_0$, $\Omega_{\mathrm{m},0}$, $c$, $\Omega_b h^2$ and $\beta$ in the IHDE IV-A (left panel) and IHDE IV-B (right panel) models

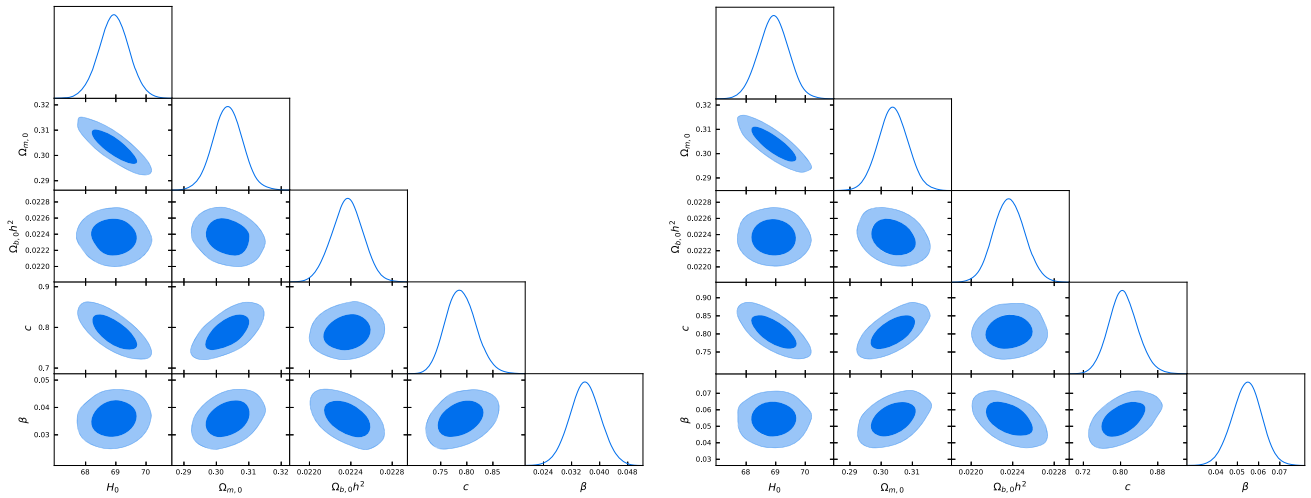


**Fig. 6** The contour plots (68.3% and 95.4% CLs) and marginalized probability distributions for the parameters $H_0$, $\Omega_{\mathrm{m},0}$, $c$, $\Omega_{\mathrm{b}} h^2$ and $\beta$ in the IHDE V-A (left panel) and IHDE V-B (right panel) models

the cosmological parameters $H_0$, $\Omega_{\mathrm{m},0}$, and $\Omega_{\mathrm{b},0}h^2$. However, all the HDE and IHDE models considered are predicted to eventually undergo the Big Rip, as $c$ remains below 1 across multiple confidence interval. Compared to the HDE model, the IHDE models yield higher central values of $c$ and exhibit a reduced statistical deviation from $c = 1$, indicating that the interaction term may help alleviate the Big Rip problem. This highlights the importance of exploring a broader range of interaction forms or alternative choices for the IR cut-off in future IHDE research. Furthermore, based on the constraints on $\beta$, we find strong support for the scenario in which DE decays into DM, reaching beyond the $7\sigma$ CL. Additionally, our results reveal a positive correlation between $c$ and $\beta$, while $H_0$ exhibits a negative correlation with $c$. The constraints on the Hubble constant show that the IHDE models have a discrepancy below $2.2\sigma$ with the Planck 2018 result [18], but exhibit a tension exceeding $3.5\sigma$ with the local measurement from Riess et al. [10]. Moreover, based on AIC, BIC, and Bayes factor, the $\Lambda$CDM model remains the best fit, while the HDE model is ruled out. In contrast, the IHDE model shows improved data fitting compared to the HDE model. Among all the IHDE models, the IHDE I-B($Q = 3\beta H_0 \rho_{\mathrm{de}}$) and IHDE V-B($Q = 3\beta H_0 \frac{\rho_{\mathrm{dm}}\rho_{\mathrm{de}}}{\rho_{\mathrm{dm}}+\rho_{\mathrm{de}}}$) models are the two most favored IHDE models based on the observational data.

As our final remarks, the $\Delta$AIC, $\Delta$BIC and $\ln B_{ij}$ values for the majority of IHDE models are nearly identical, suggesting that their fitting performances are comparable given the current dataset. This emphasizes the necessity of more precise future observations, such as a substantial dataset of gravitational wave (GW) events from binary neutron star (BNS) systems with electromagnetic (EM) counterparts. Combin-

**Table 4** Summary of model comparison results using AIC, BIC, and Bayes factor. Positive values of ΔAIC and ΔBIC, as well as negative values of ln $B_{ij}$, indicate a preference for the ΛCDM model

| Model | $\chi^2_{min}$ | ΔAIC | ΔBIC | ln $B_{ij}$ |
|---|---|---|---|---|
| ΛCDM | 1708.02 | 0 | 0 | 0 |
| HDE | 1763.49 | 57.47 | 63.00 | −31.44 |
| IHDE I-A | 1707.60 | 3.58 | 14.65 | −9.26 |
| IHDE I-B | 1706.95 | 2.93 | 14.01 | −8.59 |
| IHDE II-A | 1716.76 | 12.74 | 23.82 | −15.57 |
| IHDE II-B | 1708.61 | 4.59 | 15.67 | −9.73 |
| IHDE III-A | 1714.31 | 10.29 | 21.36 | −14.03 |
| IHDE III-B | 1707.92 | 3.89 | 14.97 | −9.49 |
| IHDE IV-A | 1709.78 | 5.76 | 16.84 | −9.84 |
| IHDE IV-B | 1707.14 | 3.12 | 14.19 | −8.33 |
| IHDE V-A | 1708.01 | 3.99 | 15.07 | −8.37 |
| IHDE V-B | 1706.68 | 2.66 | 13.73 | −7.63 |

ing these with the forthcoming complete DESI BAO dataset will be essential for effectively distinguishing between different interaction forms.

**Acknowledgements** This work was supported by the National Natural Science Foundation of China under Grants Nos. 12305056, 11505004 and 12375045, the Natural Science Foundation of Anhui Province under grant No. 1508085QA17, the Cultivation Project for Young and Middle-aged Teachers in Provincial Colleges and Universities under Grant No. YQZD2024034, and the Anhui Science and Technology University's Key Discipline Construction Fund (XK-XJGY002).

**Data Availability Statement** This manuscript has no associated data. [Authors' comment: Data sharing not applicable to this article as no datasets were generated or analysed during the current study.]

**Code Availability Statement** This manuscript has no associated code/software. [Authors' comment: Code/Software sharing not applicable to this article as no code/software was generated or analysed during the current study.]


Funded by SCOAP[3].

## References

1. A.G. Riess et al. [Supernova Search Team], Astron. J. **116**, 1009 (1998)
2. S. Perlmutter et al. [Supernova Cosmology Project Collaboration], Astron. J. **517**, 565 (1999)
3. D.N. Spergel et al., Astron. J. **148**, 175 (2003)
4. C.L. Bennett et al., Astron. J. **148**, 1 (2003)
5. M. Tegmark et al., Phys. Rev. D **69**, 103501 (2004)
6. P.J. Peebles, B. Ratra, Rev. Mod. Phys. **75**, 559 (2003)
7. S. Weinberg, Rev. Mod. Phys. **61**, 1 (1989)
8. J. Bernal, L. Verde, A. Riess, J. Cosmol. Astropart. Phys. **10**, 019 (2016)
9. L. Verde, T. Treu, A.G. Riess, Nat. Astron. **3**, 891 (2019)
10. A.G. Riess, Nat. Rev. Phys. **2**, 10 (2020)
11. E. Di Valentino et al., Astropart. Phys. **131**, 102605 (2021)
12. E. Valentino et al., Class. Quantum Gravity **38**, 153001 (2021)
13. C. Krishnan et al., Phys. Rev. D **103**, 103509 (2021)
14. L. Perivolaropoulos, F. Skara, New Astron. Rev. **95**, 101659 (2022)
15. E. Abdalla et al., J. High Energy Astrophys. **34**, 49 (2022)
16. R. Cai, Z. Guo et al., Phys. Rev. D **106**, 063519 (2022)
17. R. Cai, Z. Guo et al., Phys. Rev. D **105**, L021301 (2022)
18. N. Aghanim et al. [Planck Collaboration], Astron. & Astrophys. **641**, A6 (2020)
19. A.G. Riess et al. [Supernova Search Team], Astron. J. **934**, L7 (2022)
20. L. Amendola, Phys. Rev. D. **62**, 043511 (2000)
21. K.V. Berghaus, J.A. Kable, V. Miranda, Phys. Rev. D **110**, 103524 (2024)
22. R.R. Caldwell, Phys. Lett. B **545**, 23 (2002)
23. R. Fikri, E. ElKhateeb, E. Sayed Lashin, W. El Hanafy, (2024). arXiv:2411.19362
24. B. Feng, X. Wang, X. Zhang, Phys. Lett. B **607**, 35 (2005)
25. Y. Yang, X. Ren, Q. Wang, Z. Lu, D. Zhang, Y. Cai, E. Saridakis, Sci. Bull. **69**, 2698 (2024)
26. Y. Yang, Q. Wang, X. Ren, E. Saridakis, Y. Cai, Astrophys. J. **988**, 123 (2025)
27. A. Kamenshchik, U. Moschella, V. Pasquier, Phys. Lett. B **511**, 265 (2001)
28. S. Hussain, S. Nelleri, K. Bhattacharya, J. Cosmol. Astropart. Phys. **03**, 025 (2025)
29. M.A. van der Westhuizen, A. Abebe, J. Cosmol. Astropart. Phys. **01**, 048 (2024)
30. W. Hou, X. Zhang et al., J. Cosmol. Astropart. Phys. **05**, 017 (2023)
31. W. Yang, E. Di Valentino, S. Pan, S. Basilakos, Phys. Rev. D **102**, 063503 (2020)
32. C. Geng, C. Lee, K. Zhang, Phys. Lett. B **760**, 422 (2016)
33. C. Tzerefos, T. Papanikolaou, S. Basilakos et al., Phys. Rev. D **111**, 043523 (2025)
34. V. Poulin, T.L. Smith, T. Karwal, Phys. Dark Univ. **42**, 101348 (2023)
35. M. Bento, O. Bertolami, A. Sen, Phys. Rev. D **66**, 043507 (2002)
36. M. Hashim, A. El-Zant, Phys. Rev. D **111**, 063522 (2025)
37. M. Maggiore, M. Mancarella, Phys. Rev. D **90**, 023005 (2014)
38. S. Capozziello, A. Mazumdar, G. Meluccio, Phys. Dark Univ. **45**, 101517 (2024)
39. P. Wu, H. Yu, Phys. Lett. B **643**, 315 (2006)
40. G. Zhao, M. Raveri et al., Nat. Astron. **1**, 627 (2017)
41. S. Vagnozzi, S. Dhawan, M. Gerbino, K. Freese, Phys. Rev. D **98**, 083501 (2018)
42. J. Wang, H. Yu, P. Wu, Eur. Phys. J. C **85**, 853 (2025)
43. E.J. Copeland, M. Sami, S. Tsujikawa, Int. J. Mod. Phys. D **15**, 1753 (2006)
44. N. Frusciante, L. Perenon, Phys. Rep. **857**, 1 (2020)
45. P. Bull et al., Phys. Dark Univ. **12**, 56 (2016)
46. G. 't Hooft, (1993). arXiv:gr-qc/9310026
47. A.G. Cohen, D.B. Kaplan, A.E. Nelson, Phys. Rev. Lett. **82**, 4971 (1999)

48. S.D.H. Hsu, Phys. Lett. B **594**, 13 (2004)
49. M. Li, Phys. Lett. B **603**, 1 (2004)
50. R. Horvat, Phys. Rev. D **70**, 087301 (2004)
51. Q.G. Huang, M. Li, J. Cosmol. Astropart. Phys. **03**, 001 (2005)
52. H.C. Kao, W.L. Lee, F.L. Lin, Phys. Rev. D **71**, 123518 (2005)
53. H. Kim, H.W. Lee, Y.S. Myung, Phys. Lett. B **632**, 605 (2006)
54. H. Li, Z. Guo, Y. Zhang, Int. J. Mod. Phys. D **15**, 869 (2006)
55. X. Zhang, F.Q. Wu, Phys. Rev. D **76**, 023502 (2007)
56. M. Li, X.D. Li, S. Wang, X. Zhang, J. Cosmol. Astropart. Phys. **06**, 036 (2009)
57. Y. Gong, T. Li, Phys. Lett. B **683**, 241 (2010)
58. J. Cui, X. Zhang, Phys. Lett. B **690**, 233 (2010)
59. S. Del Campo, J.C. Fabris et al., Phys. Rev. D **83**, 123006 (2011)
60. T. Naderi, M. Malekjani, F. Pace, MNRAS. **447**, 1873 (2015)
61. S. Nojiri, S.D. Odintsov, Eur. Phys. J. C **77**, 528 (2017)
62. M. Malekjani, M. Rezaei, I.A. Akhlaghi, Phys. Rev. D **98**, 063533 (2018)
63. H. Moradpour, S.A. Moosavi et al., Eur. Phys. J. C **78**, 829 (2018)
64. B.D. Pandey, P.S. Kumar, S. Pankaj, Eur. Phys. J. C **82**, 233 (2022)
65. Q.G. Huang, Y. Gong, J. Cosmol. Astropart. Phys. **08**, 006 (2004)
66. J. Shen, B. Wang, E. Abdalla, R.K. Su, Phys. Lett. B **609**, 200 (2005)
67. X. Zhang, F.Q. Wu, Phys. Rev. D **72**, 043524 (2005)
68. Z. Chang, F.Q. Wu, X. Zhang, Phys. Lett. B **633**, 14 (2006)
69. M. Li, X.D. Li, J. Cosmol. Astropart. Phys. **12**, 014 (2009)
70. Y.Z. Ma, Y. Gong et al., Eur. Phys. J. C **60**, 303 (2009)
71. X. Zhang et al., Phys. Lett. B **683**, 81 (2010)
72. B. Wang, C.Y. Lin et al., Phys. Lett. B **637**, 357 (2006)
73. H. Mohseni Sadjadi, M. Honardoost, Phys. Lett. B. **647**, 231 (2007)
74. J. Zhang, X. Zhang et al., Phys. Lett. B **659**, 26 (2008)
75. B. Wang, C.Y. Lin, D. Pavón, E. Abdalla, Phys. Lett. B **662**, 1 (2008)
76. K. Karwan, J. Cosmol. Astropart. Phys. **05**, 011 (2008)
77. H. Mohseni Sadjadi, Eur. Phys. J. C. **62**, 419 (2009)
78. M. Sharif, A. Jawad, Eur. Phys. J. C **72**, 2097 (2012)
79. S. Wang, Y. Wang, M. Li, Phys. Rep. **696**, 1 (2017)
80. E. Sadri, M. Khurshudyan et al., Eur. Phys. J. C **80**, 393 (2020)
81. R.G. Landim, Phys. Rev. D **106**, 043527 (2022)
82. M. Li, C. Lin, Y. Wang, J. Cosmol. Astropart. Phys. **05**, 023 (2008)
83. D. Pavón, W. Zimdahl, Phys. Lett. B **628**, 206 (2005)
84. I. Durán, D. Pavón, W. Zimdahl, J. Cosmol. Astropart. Phys. **07**, 018 (2010)
85. Z. Zhang, S. Li, X.-D. Li, X. Zhang, M. Li, J. Cosmol. Astropart. Phys. **06**, 009 (2012)
86. L. Feng, X. Zhang, J. Cosmol. Astropart. Phys. **08**, 072 (2016)
87. H. Li, J. Zhang, L. Feng, X. Zhang, Eur. Phys. J. C **77**, 907 (2017)
88. A. Lewis, S. Bridle, Phys. Rev. D **66**, 103511 (2002)
89. A. Gelman, D.B. Rubin, Stat. Sci. **7**, 457 (1992)
90. M. Abdul Karim et al. [DESI Collaboration], (2025). arXiv:2503.14738
91. M. Abdul Karim et al. [DESI Collaboration], (2025). arXiv:2503.14739
92. A. Brodzeller et al. [DESI Collaboration], (2025). arXiv:2503.14740
93. U. Andrade et al. [DESI Collaboration], (2025). arXiv:2503.14742
94. T.M.C. Abbott et al. [DES Collaboration], Astron. J. **973**, L14 (2024)
95. A.G. Adame et al. [DESI Collaboration], J. Cosmol. Astropart. Phys. **04**, 012 (2025)
96. A.G. Adame et al. [DESI Collaboration], J. Cosmol. Astropart. Phys. **01**, 124 (2025)
97. A.G. Adame et al. [DESI Collaboration], J. Cosmol. Astropart. Phys. **02**, 021 (2025)
98. S. Chen et al., Mon. Not. R. Astron. Soc. **534**, 544 (2024)
99. A. Favale, A. Gómez-Valent et al., Phys. Lett. B **858**, 139027 (2024)
100. U. Tyagi, S. Haridasu, S. Basak, Phys. Rev. D **110**, 063503 (2024)
101. S. Yuan, 50 colleagues, Mon. Not. R. Astron. Soc. **533**, 589 (2024)
102. B. Dinda, J. Cosmol. Astropart. Phys. **09**, 062 (2024)
103. J. Wang, Z. Huang, Y. Yao, J. Liu, L. Huang, Y. Su, J. Cosmol. Astropart. Phys. **09**, 053 (2024)
104. A. Anand et al., Astron. J. **168**, 124 (2024)
105. Y. Tada, T. Terada, Phys. Rev. D **109**, L121305 (2024)
106. F. Yang, X. Fu et al., Eur. Phys. J. C **85**, 186 (2025)
107. L. Huang, R. Cai, S. Wang, (2025). arXiv:2502.04212
108. W. Guo, Q. Wang et al., Astrophys. J. **978**, L33 (2025)
109. J. Pan, G. Ye, (2025). arXiv:2503.19898
110. A. Ormondroyd, W.J. Handley et al., (2025). arXiv:2503.17342
111. L. Anchordoqui, I. Antoniadis, D. Lust, (2025). arXiv:2503.19428
112. S. Nakagawa, Y. Nakai et al., (2025). arXiv:2503.18924
113. T. Li, Y. Li et al., Eur. Phys. J. C **85**, 608 (2025)
114. J. Li, S. Wang, J. Cosmol. Astropart. Phys. **07**, 047 (2025)
115. D. Eisenstein et al., Astrophys. J. **633**, 560 (2005)
116. D. Eisenstein, W. Hu, Astrophys. J. **496**, 605 (1998)
117. A. Lewis, A. Challinor, A. Lasenby, Astrophys. J. **538**, 473 (2000)
118. Aubourg et al. [BOSS Collaboration], Phys. Rev. D **92**, 123516 (2015)
119. Z. Zhai, C. Park, Y. Wang, B. Ratra, J. Cosmol. Astropart. Phys. **07**, 009 (2020)
120. L. Chen, Q. Huang, K. Wang, J. Cosmol. Astropart. Phys. **02**, 028 (2019)
121. Z. Zhai, Y. Wang, J. Cosmol. Astropart. Phys. **07**, 005 (2019)
122. A. Conley et al., ApJS. **192**, 1 (2011)
123. W. Hu, N. Sugiyama, Astrophys. J. **471**, 542 (1996)
124. K. Zhang, T. Zhou, B. Xu, Q. Huang, Y. Yuan, Astrophys. J. **957**, 5 (2023)
125. R. Jimenez, A. Loed, Astrophys. J. **573**, 37 (2002)
126. M. Moresco, R. Jimenez, L. Verde, Astrophys. J. **898**, 82 (2020)
127. H. Akaike, IEEE Trans. Autom. Control **19**, 716 (1974)
128. G. Schwarz, Estimating the dimension of model. Ann. Stat. **6**, 461 (1978)
129. R. Trotta, Contemp. Phys. **49**, 71 (2008)
130. R.E. Kass, A.E. Raftery, J. Am. Stat. Assoc. **90**, 773 (1995)
131. W. Handley, M. Hobson, A. Lasenby, Mon. Not. R. Astron. Soc. **450**, L61 (2015)
132. W. Handley, M. Hobson, A. Lasenby, Mon. Not. R. Astron. Soc. **453**, 4384 (2015)